Genome-wide evidence of the role of Paf1C in transcription elongation and histone H2B monoubiquitination in *Arabidopsis*

Noel Blanco-Touriñán[1,#], Jaime Pérez-Alemany[1,#], Clara Bourbousse[2], David Latrasse[3], Ouardia Ait-Mohamed[2], Moussa Benhamed[3], Fredy Barneche[2], Miguel A. Blázquez[1], Javier Gallego-Bartolomé[1], David Alabadí[1,*]

[1]Instituto de Biología Molecular y Celular de Plantas (CSIC-UPV), Valencia (Spain)
[2]Institut de Biologie de l'Ecole Normale Supérieure (CNRS), Ecole normale supérieure, CNRS, INSERM, Université PSL, Paris, France
[3]Institute of Plant Sciences Paris-Saclay (Université Paris-Saclay-CNRS), Orsay (France)

[#]Noel Blanco-Touriñán and Jaime Pérez-Alemany contributed equally to this work
*Correspondence: David Alabadí (dalabadi@ibmcp.upv.es)

Running head: Role of Paf1C in transcriptional elongation

Abstract

The evolutionarily conserved Paf1 complex (Paf1C) participates in transcription, and research in animals and fungi suggests that it facilitates RNAPII progression through chromatin remodeling. To obtain evidence that Paf1C acts in transcription elongation in *Arabidopsis*, we examined the genomic distribution of the ELF7 and VIP3 subunits of Paf1C. The occupancy of both subunits was confined to thousands of gene bodies and positively correlated with RNAPII occupancy and the level of gene expression, supporting a role as a transcription elongation factor. We found that monoubiquitinated histone H2B, which marks most transcribed genes, was strongly reduced genome-wide in *elf7* seedlings. Genome-wide profiling of RNAPII revealed that in *elf7* mutants, RNAPII occupancy was reduced throughout the gene body and at the transcription end site of Paf1C-targeted genes, suggesting a direct role for the complex in transcription elongation. Overall, our observations suggest that there is a direct functional link between Paf1C activity, mono-ubiquitination of histone H2B, and the transition of RNPII to productive elongation. However, for several genes, Paf1C may also act independently of H2Bub deposition or occupy these genes more stably than H2Bub marking, possibly reflecting the dynamic nature of Paf1C association and H2Bub turnover during transcription.

30 **INTRODUCTION**

31 During gene transcription, numerous proteins and protein complexes help RNA
32 Polymerase II (RNAPII) to move through the gene body, including histone chaperones,
33 chromatin remodelers, and transcription elongation factors, most of which are
34 evolutionarily conserved in eukaryotes (Obermeyer et al., 2023). One of them is the
35 transcription elongation complex POLYMERASE ASSOCIATED FACTOR1 (Paf1C). Paf1C
36 was originally identified in yeast and the current view of how Paf1C acts in gene
37 regulation is largely based on studies in yeast and mammals (Francette et al., 2021).
38 Early genetic and biochemical evidence for a positive role of Paf1C in transcriptional
39 elongation (Shi et al., 1997; Rondón et al., 2004) is now supported by structural studies
40 showing the association of the complex with active RNAPII (Vos et al., 2018; Vos et al.,
41 2020). Paf1C is also involved in posttranslational modification of histones. Histone
42 modifications such as the monoubiquitination of histone H2B (H2Bub) or the
43 methylation of lysines 4 or 36 of histone H3 (H3K4me, H3K36me), which influence
44 chromatin dynamics co-transcriptionally to facilitate RNAPII progression, have been
45 found to be dependent on Paf1C in yeast and mammals (Francette et al., 2021).

46 Several subunits of plant Paf1C have been genetically identified in *Arabidopsis* in
47 genetic screens for early flowering mutants or by searching for homologous genes
48 (Zhang and Van Nocker, 2002; Zhang et al., 2003; He et al., 2004; Oh et al., 2004; Park
49 et al., 2010; Yu and Michaels, 2010). As in animals, the plant Paf1C contains six subunits,
50 PLANT HOMOLOGOUS TO PARAFIBROMIN (PHP)/CELL DIVISION CYCLE73 (CDC73),
51 VERNALIZATION INDEPENDENCE2 (VIP2; also known as EARLY FLOWERING7, ELF7),
52 VIP3, VIP4, VIP5, and VIP6 (ELF8), which are the putative orthologs of CDC73, Paf1, SKI8,
53 LEO1, RTF1, and CTR9, respectively (Obermeyer et al., 2023). The *Arabidopsis* Paf1C is
54 formed *in vivo*, since at least VIP3, VIP4, and VIP6 interact with PHP/CDC73 (Park et al.,
55 2010) and all subunits were identified in interactomic analyses using CDC73 and ELF7 as
56 baits (Antosz et al., 2017). Furthermore, the latter study showed that Paf1C interacts
57 with *bona fide* transcriptional elongation factors and with several subunits of RNAPII,
58 pointing to a conserved role in transcriptional elongation.

59 In addition to flowering, and consistent with the pleiotropic effects of loss-of-
60 function mutants in several subunits, plant Paf1C has been associated genetically with a
61 variety of largely unrelated physiological processes in *Arabidopsis*, including seed

62 dormancy (Liu et al., 2011), shoot apical meristem activity (Fal et al., 2017; Fal et al.,
63 2019; Li et al., 2022), thermomorphogenesis (Zhao et al., 2023), and the response to salt
64 stress (Zhang et al., 2022) and DNA damaging agents (Li et al., 2023).

65 In *Arabidopsis*, the role of Paf1C in post-translational modification of histones is
66 well-documented and has been associated with several physiological processes. This
67 includes the regulation of flowering time by acting on the flowering repressor gene
68 *FLOWERING LOCUS C* (*FLC*) and its paralogs (Cao et al., 2015; Lu et al., 2017; Li et al.,
69 2019; Nasim et al., 2022). The requirement of Paf1C for histone modifications has also
70 been shown at the epigenomic level. Although the total amount of H3K4me3 and
71 H3K36me2 marks is not altered in *vip3*, *vip4*, *vip5*, or *vip6* cell extracts (Oh et al., 2004),
72 the *vip3* mutation triggers a slight redistribution of both marks across gene bodies (Oh
73 et al., 2008). Moreover, plant Paf1 subunits are required for the correct distribution of
74 H2A.Z and H3.3 in response to warm temperatures (Zhao et al., 2023) and for regulating
75 H3K27 trimethylation at a subset of genes (Oh et al., 2008; Schmitz et al., 2009).

76 In line with the role of Paf1C in animals and fugi in promoting H2Bub accumulation,
77 mutations in *Arabidopsis VIP2, VIP4, VIP5,* and *VIP6* subunits cause decreased H2Bub
78 accumulation at *FLC* and its paralog genes (Cao et al., 2015). More recently, the
79 dependence of H2Bub on Paf1C has been linked to the DNA damage response (Li et al.,
80 2023). In *Arabidopsis*, as in yeast and animals, H2Bub accumulates across the gene
81 bodies of actively transcribed genes (Roudier et al., 2011; Bourbousse et al., 2012;
82 Nassrallah et al., 2018). However, it is not known whether Paf1C is present at many
83 transcribed genes where it might contribute to H2Bub deposition or whether it
84 indifferently affects this mark at all *loci*. To gain insight into transcription-associated
85 chromatin mechanisms and their regulatory roles in plant development and stress
86 responses, we here examined the involvement of Paf1C in transcription elongation by
87 RNAPII and in monoubiquitination of histone H2Bub throughout the *Arabidopsis*
88 genome.

89

90 **RESULTS**

91 **The subunits of Paf1C ELF7 and VIP3 are recruited to gene bodies**

92 First, we investigated the genomic distribution of Paf1C by profiling the chromatin
93 association of the ELF7 and VIP3 subunits by ChIP-seq in one-week-old *Arabidopsis*

94 seedlings. ChIP-seq analyses were performed using the *Flag-ELF7* and *GFP-VIP3*
95 transgenic lines, respectively (Dorcey et al., 2012; Cao et al., 2015) and non-transgenic
96 WT plants as negative controls. The resulting analysis indicated a high correlation
97 between biological replicates (Fig. S1, A and B) and identified 9,791 and 6,845 Flag-ELF7
98 and GFP-VIP3 peaks, respectively (usually one peak per protein-coding gene; see
99 examples in Fig. S1C), of which the vast majority was common (Fig. 1, A and B and
100 Supplemental Table). A heatmap representation of Flag-ELF7 and GFP-VIP3 ChIP signal
101 over unique and shared targeted genes confirmed that most of them were in fact bound
102 by both proteins, albeit with different intensities (Fig. S2A). Thus, for the next analyses
103 we considered all the peaks identified for the two subunits as *bona fide* Paf1C target loci
104 (10,579) (Fig. 1A).

105 The genomic profile of Paf1C showed a strongest enrichment over gene bodies that
106 slightly extends in 3' over the transcription end site (TES) (Fig. 1, B-D, and Fig. S2A).
107 Comparison with RNAPII profiles showed that the overlap of the distributions of Paf1C
108 and RNAPII was restricted to gene bodies (Fig. 1B). The ELF7 distribution observed in this
109 work was very similar to that found in a recent study (Fig. S2B) (Wang et al., 2023b). In
110 accordance with Paf1C's role in transcription elongation, the occupancy of ELF7 and VIP3
111 exhibited a positive correlation with RNAPII occupancy (Fig. S1B) and transcript levels
112 (Fig. 1, C and D). To further substantiate this perspective, we examined the accumulation
113 of different histone marks and histone variants at Paf1C target genes (Jamge et al.,
114 2023). Paf1C target genes were enriched in histone marks associated with active gene
115 transcription, such as H3K4me3 and H3K36me3, while being depleted of the *Polycomb*-
116 based H3K27me3 mark (Fig. S2A). Also consistent with Paf1C being associated with
117 expressed genes and not with *Polycomb*-repressed genes, histone variant H2A.Z was
118 enriched at the 5' end but mostly absent across the gene bodies of Paf1C targets (Fig.
119 S2A) (Coleman-Derr and Zilberman, 2012; Gómez-Zambrano et al., 2019).

120 To investigate the impact of Paf1C depletion on gene expression, we determined
121 the transcriptome in wild-type and *elf7-3* one-week-old seedlings by RNA-seq. We
122 identified 4,002 differentially expressed genes (DEGs; p adj. < 0.05) in *elf7-3* seedlings
123 (Fig. 1, E and F, and Supplemental Table). More than half of the identified DEGs (2,265)
124 were *bona fide* Paf1C targets (Fig. 1E and Fig. S2C). Interestingly, when we plotted the
125 average signal of Flag-ELF7 or GFP-VIP3 across DEGs in the "Other expressed" category

126 (Fig. 1F), we found enrichment in gene bodies for both subunits compared with gene
127 bodies of non-expressed genes, which correlates with the RNAPII signal (Fig. S2C). This
128 result suggests that the DEGs of the "Other expressed" category are also target genes
129 of Paf1C, although they are only weakly bound by the complex in accordance with their
130 low expression level. The weak binding may be the reason that these genes were below
131 the threshold to be detected by peak calling as true Paf1C targets. In any case, the DEGs
132 represent a fraction of all loci bound to Paf1C in the genome, a situation similar to that
133 observed in human cells knocked-down for the ortholog Paf1 subunit (Yu et al., 2015).
134 Among the *bona fide* Paf1C target DEGs, 1,040 were downregulated consistent with a
135 positive role of the complex on transcription elongation. Intriguingly, 1,225 DEGs were
136 upregulated in the mutant, suggesting a negative impact of Paf1C on their expression or
137 the existence of indirect effects mediating their induction in the absence of Paf1C.
138
139 **Defects in the Paf1C complex affect H2Bub mark genome-wide**
140 Paf1C is required for efficient monoubiquitination of H2B in various organisms, including
141 plants (Wood et al., 2003; Schmitz et al., 2009; Hou et al., 2019; Li et al., 2023). To
142 determine whether reduction of H2Bub deposition is detected at specific genes or on a
143 global scale along the genome upon Paf1C loss-of-function, we examined the H2Bub
144 dependence in wild-type and *elf7-3* seedlings by ChIP-seq with spike-in of exogenous
145 chromatin (ChIP-Rx). Following the protocol described in Nassrallah et al. (2018) for
146 *Arabidopsis*, spike-in based normalization enables for accurate quantitative
147 comparisons of samples with genome-wide differences in chromatin mark abundances
148 In our analyses, H2Bub was exclusively enriched in the transcribed regions (Fig. 2, A and
149 B), in agreement with previous reports in *Arabidopsis* (Roudier et al., 2011; Bourbousse
150 et al., 2012; Nassrallah et al., 2018). In addition, H2Bub-occupied genes were also co-
151 ocupied by Paf1C and RNAPII (Fig. S3A), as expected for a co-transcriptionally deposited
152 mark.
153 In the absence of Paf1C, H2Bub levels were strongly affected at multiple genes (Fig.
154 2, A and B, and Fig. S3, B and C). More precisely, identification of differentially
155 ubiquitinated genes showed a general tendency for reduced H2Bub enrichment over
156 most H2Bub-marked genes in *elf7-3* seedlings (Fig. 2C and Supplemental Table). Hence,
157 given the frequent local co-occurrence of Flag-ELF7/GFP-VIP3 and the H2Bub mark,

158 these observations suggest the existence of direct functional links between Paf1c
159 activity and histone H2B monoubiquitination.

160 However, the association of Flag-ELF7 and GFP-VIP3 with chromatin was also found
161 in genes enriched in RNAPII but not H2Bub (Fig. 2B, and Fig. S3C and Supplemental
162 Table). We found that these genes were smaller compared with the genes that were co-
163 ocuppied by Paf1C and H2Bub (Fig. S3D). As previously identified using transcriptome
164 data (Bourbousse et al., 2012), this observation suggests that optimal transcription of
165 small genes in *Arabidopsis* is less dependent on H2Bub. Furthermore, it indicates that
166 Paf1C may function independently of H2Bub deposition at multiple genes or that it may
167 occupy these genes more persistently than H2Bub. *Vice versa*, H2Bub enrichment was
168 detected at genes in which we could not detect Paf1C (Fig. 2B). Interestingly, H2Bub was
169 also reduced at these genes in *elf7-3* seedlings, possibly indicating that Paf1C acted on
170 histone H2B monoubiquitination transiently, or earlier, at these loci. In summary, these
171 observations suggest that histone H2B monoubiquitination is tightly linked to Paf1C
172 activity at many genes but may also reflect the dynamic nature of Paf1C association
173 dynamics and H2Bub turn-over during transcription. However, we cannot exclude that
174 the lack of a complete correlation between the presence of Paf1C and the H2Bub mark
175 observed in some of these genes may be due to technical limitations linked to stringent
176 peak calling for detecting them or to Paf1C-independent H2Bub dynamics.

177 The H2Bub mark preferentially accumulates in longer genes in *Arabidopsis* (Fig. S3D)
178 (Roudier et al., 2011). In addition, in mouse muscle myoblast cells loss of Paf1C reduces
179 H2Bub mark over the 5' of long genes, while the entire gene body is affected in medium
180 and small size genes (Hou et al., 2019). On this basis, we decided to determine whether
181 the requirement of Paf1C for histone H2B monoubiquitination is affected by gene size
182 in plants. We ranked the H2Bub- and Paf1C-marked genes by gene size and compared
183 the H2Bub signal in wild-type and *elf7-3* seedlings. This showed that the impact of Paf1C
184 on H2Bub level is independent of gene size in *Arabidopsis* (Fig. S4).

185 Studies in yeast and mammals provided molecular insights into the functional
186 relationship between Paf1C and histone H2B monoubiquitination by the E2 conjugating
187 enzyme Rad6 and the E3 ligase Bre1 in yeast and RNF20/RNF40 in mammals. In yeast,
188 Paf1C promotes monoubiquitination through direct interaction with Rad6/Bre1 and
189 does not appear to affect Rad6 recruitment to chromatin (Ng et al., 2003; Wood et al.,

190 2003; Kim and Roeder, 2009), whereas in mammals, RNF20/40 recruitment to
191 chromatin is dependent on Paf1C (Wu et al., 2014). To investigate the situation in
192 *Arabidopsis*, we examined whether the reduction in H2Bub mark in the *elf7-3* mutant
193 was due to impaired recruitment to chromatin of HISTONE MONOUBIQUITINATION1
194 (HUB1) and HUB2, the two E3 ubiquitin ligases mediating H2Bub deposition in
195 *Arabidopsis* (Liu et al., 2007). To this end, we fractionated cell extracts of the wild type
196 and the *elf7-3* mutant and used a custom-made antibody to determine HUB1/2 levels
197 (Fig. 3A) and their association with chromatin compared with cytoplasmic and
198 nucleoplasmic fractions by immunoblotting. We observed a band corresponding to
199 HUB1/2 in the chromatin fraction of wild-type cell extracts, and these levels were not
200 affected by the *elf7-3* mutation (Fig. 3B). This result suggests that Paf1C promotes
201 histone H2B monoubiquitination independently of HUB1/2 recruitment to chromatin in
202 *Arabidopsis*.
203
204 **Paf1C and histone H2B monoubiquitination regulate common processes**
205 The functional relationship between Paf1C and H2Bub should manifest itself in common
206 DEGs in mutants defective for Paf1C or for the machinery that monoubiquitinates
207 histone H2B. We compared the transcriptomes of *elf7-3* and *hub1-4* mutant (Liu et al.,
208 2007) seedlings grown side-by-side. We identified 413 DEGs (p adj. < 0.05) in *hub1-4*
209 seedlings, a reduced number compared to *elf7-3* (Fig. 4, A and B). More than half of
210 DEGs in *hub1-4* were also misregulated in *elf7-3* seedlings (Fig. 4B) and, importantly, this
211 subset showed the same trend in gene expression change, in line with the functional
212 link between Paf1C and H2Bub (Fig. 4, C and D). The majority of DEGs in *hub1-4* and
213 those common to both mutants were occupied by Paf1C (Fig. S5), suggesting direct
214 functional links between Paf1C and H2Bub in gene expression.
215
216
217 ***elf7* mutation causes RNAPII stalling at the 5' end of genes**
218 We next examined the effect of impaired Paf1C on RNAPII occupancy. ChIP-seq profiling
219 of the NRPB1 subunit, which indiscriminately captures all active RNAPII states, detected
220 peaks at 18,339 genes, half of which were also occupied by Paf1C. In wild-type plants,
221 RNAPII distribution showed a typical pattern with peaks immediately after the

222 transcription start site (TSS) and at the TES and lower levels throughout the gene body,
223 where RNAPII processivity is high and residence time is low (Figs. 1B, 2B, and 5A). The
224 peak after the TSS reflected RNAPII stalled at the +1 nucleosome (Fig. 5B), as previously
225 reported (Kindgren et al., 2019). Importantly, we observed a redistribution of RNAPII
226 signal in the *elf7-3* mutant compared with wild type plants, with reduced accumulation
227 over gene bodies and TES and increased accumulation across the TSS region (Fig. 5, A
228 and C). Overall, these defects most likely reflect a more frequent stalling of RNAPII in
229 *elf7-3* plants.

230 Several lines of evidence pointed to a direct contribution of Paf1C to RNAPII
231 redistribution. Reduction of RNAPII occupancy at gene bodies and TES in *elf7-3* seedlings
232 was observed preferentially for Paf1C target genes (Fig. 5C). This suggests that Paf1C
233 contributes locally to transcription elongation. Indeed, Paf1C target genes were
234 enriched in histone marks associated with active transcription (Fig. 5C and Fig. S2A).
235 However, the increased accumulation of RNAPII at TSS observed in *elf7-3* seedlings also
236 occurred in genes where no Paf1C peak was detected (Fig. 5C). This result suggests that
237 the effect of the *elf7-3* mutation on stalled RNAPII may result from direct and indirect
238 consequences of defective Paf1C, such as reduced H2B monoubiquitination (Fig. 5C).
239 Interestingly, the accumulation of stalled RNAPII in *elf7-3* mutant plants was shifted
240 toward the 5' end of the genes compared with wild type (Fig. 5B). However, it is unclear
241 whether this shift is due to the +1 nucleosome moving toward the 5' end of the genes
242 in the mutant.

243 Finally, the possibility that Paf1C is involved in transcription elongation was further
244 supported by comparing the RNAPII pausing index of wild-type and *elf7-3* mutant plants.
245 Similar to previous studies (Wang et al., 2023a), we calculated the pausing index as the
246 ratio of RNAPII occupancy across the TSS to RNAPII occupancy in the gene body (Fig. 5D).
247 As shown in Fig. 5E, the RNAPII pausing index increased in plants of the Paf1C mutant.
248 This is consistent with the idea that Paf1C contributes to the productive elongation of
249 RNAPII.

250

251 **DISCUSSION**

252 In this study, we provide genome-wide evidence for the function of Paf1C as a
253 transcriptional elongation factor in plants. First, the Paf1C subunits ELF7 and VIP3 are

254 exclusively distributed in gene bodies and their accumulation positively correlates with
255 that of RNAPII and gene expression, suggesting that the complex actively promotes gene
256 transcription (Fig. 1, B-D and Fig. S2). Second, monoubiquitination of histone H2B, a
257 chromatin mark that is deposited co-transcriptionally, is severely reduced in virtually all
258 genes in Paf1C-defective plants, a defect that is particularly pronounced in Paf1C-
259 targeted genes (Figs. 2 and 4C). Third, RNAPII appears to stall more frequently at the 5'
260 end of genes, and the overall gene body occupancy is reduced in Paf1C-targeted genes
261 in *elf7-3* mutant plants (Fig. 4A-C). This likely reflects the inability of RNAPII to transition
262 to the productive elongation stage. The latter is consistent with previous results in
263 *Arabidopsis*, which demonstrate that (i) the phosphorylated form of RNAPII at serine 5
264 (Ser5) of the C-terminal domain of NRPB1 (RNAPII-Ser5), marking engaged RNAPII,
265 accumulates in the *elf7-3* mutant around the TSS (Wang et al., 2023b); and (ii) the
266 occupancy at gene bodies of Ser2 phosphorylated RNAPII, the elongating form, is
267 reduced in the *elf7-3* mutant (Obermeyer et al., 2022).

268 Despite this evidence for a role of Paf1C in transcription elongation, we still lack
269 information on the mechanism of action of this complex in plants. In this regard, a
270 comparison of the genomic distribution of Paf1C and RNAPII in different model
271 organisms could provide relevant information. The genomic profile of the *Arabidopsis*
272 Paf1C subunits ELF7 and VIP3 strongly resembles that of the Paf1 subunit in yeast, as
273 both are mainly localized within the gene bodies (Fig. 1, B and C) (Mayer et al., 2010;
274 Wang et al., 2023b). It is noteworthy, however, that while RNAPII, much like Paf1C, is
275 found within gene bodies, their distributions do not entirely overlap, as RNAPII exhibits
276 heightened enrichment at the TSS and TES (Figs. 1B and 5B). In mammals, the
277 distribution of Paf1C parallels the distribution of RNAPII, as both are enriched across the
278 TSS and after the TES (Rahl et al., 2010; Chen et al., 2015; Yu et al., 2015). In mammals,
279 their similar distributions therefore reflect an association of Paf1C with RNAPII, with
280 Paf1C involved in the regulation of RNAPII pausing immediately after the TSS (Chen et
281 al., 2015; Yu et al., 2015) and contributing to mRNA polyadenylation (Nagaike et al.,
282 2011). However, in *Arabidopsis*, the genes are generally much shorter than in mammals.
283 Consistent with the positive correlation observed in mammals between the distribution
284 of Paf1C and RNAPII, the accumulation of Paf1C at gene bodies in *Arabidopsis* may be
285 important for productive transcription elongation, as shown in Fig. 5C. Consistent with

286 this possibility, RNAPII accumulates near the TSS of genes and is locally shifted toward
287 5', whereas the RNAPII pausing index is increased in the *elf7* mutant compared with
288 wild-type plants.

289 How does Paf1C contribute to transcriptional elongation? The association of Paf1C
290 with RNAPII could facilitate the passage of the transcriptional machinery through the
291 nucleosomes through several mechanisms. Structural studies in mammals have shown
292 that Paf1C position in the RNAPII transcriptional complex should enable it to promote
293 methylation of histone H3K4 in downstream nucleosomes -a modification known to
294 facilitate transcription (Vos et al., 2018). We hypothesize that Paf1C would be recruited
295 to RNAPII positioning itself within the complex similarly to its mammalian counterpart.
296 Subsequently, Paf1C would promote post-translational modifications of histones such
297 as monoubiquitination of H2B in nucleosomes downstream of the +1, thereby
298 facilitating the passage of RNAPII thoughout the whole gene body where we found both
299 Paf1C and H2Bub to frequently accumulate. The direct effect of Paf1C on local HUB1/2
300 activity is supported by several observations in this study, including the frequent co-
301 occupancy of genes by Paf1C and RNAPII, with high levels of H2Bub in this context, the
302 association of HUB1/2 with chromatin even in the absence of Paf1C, and the previously
303 described physical interaction between the Paf1C subunit VIP5 and the *Arabidopsis*
304 homologs of the Rad6 E2 ubiquitin-conjugating enzyme (Li et al., 2023). Nevertheless,
305 the reduced H2Bub deposition in *elf7* mutant plants could in some cases result from
306 indirect effects of Paf1C deficiency, such as impaired RNAPII elongation.
307
308

309 **MATERIALS AND METHODS**

310 **Plant material.**

311 The *Arabidopsis* lines used in this work have been previously described: *elf7-3* (He et al.,
312 2004), *hub1-4* and *hub1-3 hub2-2* (Liu et al., 2007), *pELF7:Flag-ELF7 elf7-3* (Cao et al.,
313 2015), and *35S:GFP-VIP3* (Dorcey et al., 2012).
314

315 **Growth conditions and treatments**

316 All seeds were surface sterilized and sown on half-strength MS (Duchefa) plates
317 containing 1% (w/v) sucrose, 8 g/L agar (pH 5.7). Seedlings were grown at 22ºC under
318 continuous light (50-60 µmol m^{-2} s^{-1}) (standard conditions).
319
320 **RNA-seq experiments**
321 RNA-seq with three independent biological replicates for each genotype were
322 performed. Seedlings were grown as described above. 7-day-old wild type, *elf7-3*, and
323 *hub1-4* seedlings were collected. Total RNA was extracted using an RNeasy Plant Mini
324 Kit (Qiagen) according to the manufacturer´s instructions. RNA concentration and
325 integrity were measured in an RNA Nanochip (Bioanalyzer, Agilent Technologies 2100)
326 from IBMCP Genomics Service. Library preparation and sequencing were performed by
327 the Genomics Service of the University of Valencia.
328
329 **RNA-seq analysis**
330 RNA-seq read quality was first evaluated using FastQC v0.11.9. Low-quality bases and
331 Illumina adapters were trimmed using cutadapt v4.2 with options "-q 15,10 -a
332 AGATCGGAAGAGCACACGTCTGAACTCCAGTCA -m 20 --trim-n". Clean reads were then
333 aligned to the TAIR10 reference genome using STAR v2.7.10b (Dobin et al., 2013) with
334 the default parameters. Read counts were obtained using the featureCounts command
335 from subread v2.0.3 (Liao et al., 2014) with the default parameters and providing the
336 Araport11 annotation. Differential analyses were performed using DESeq2 v1.38 (Love
337 et al., 2014). Genes showing an adjusted p-value inferior to 0.05 were considered as
338 differentially expressed.
339
340 **ChIP experiments**
341 H2B and H2Bub ChIP-Rx were performed in parallel with the same two biological
342 replicates of 7-day-old wild-type and *elf7-3* seedlings grown under standard conditions.
343 As previously described (Nassrallah et al., 2018), all samples were spiked-in with
344 *Drosophila* chromatin prior to IP. The amount of exogenous DNA was subsequently
345 determined in all input and IP samples and considered as a reference to avoid the effects
346 of technical variation. Furthermore, we determined the H2Bub peaks after
347 normalization to histone H2B occupancy determined in the same samples by ChIP-Rx.

348 Specifically, for each biological replicate, two IPs were performed with an anti-H2Bub
349 antibody (MM -0029-P, Medimabs) and one with an anti-H2B (ab1790, Abcam). For each
350 IP, 100 µg of *Arabidopsis* chromatin mixed with 3 µg of *Drosophila* chromatin was used.
351 DNA eluted from the two technical replicates of the H2Bub IP was pooled prior to library
352 preparation. Library preparation and sequencing was performed by the CRG Genomics
353 Core Facility (Barcelona, Spain). Flag-ELF7 and GFP-VIP3 ChIP-seqs were performed
354 using 7-day-old seedlings grown under standard conditions and an anti-Flag M2
355 antibody (F1804, Sigma) and an anti-GFP antibody (ab290, abcam), respectively. We
356 used double in vitro cross-linking with 1.5 mM ethylene glycol bis (succinimidyl
357 succinate) for 20 minutes followed by 1% formaldehyde for 10 minutes at room
358 temperature. Library preparation and sequencing were performed by the CRG Genomics
359 Core Facility (Barcelona, Spain). ChIP-seq for RNAPII was performed using an anti-RPB1
360 antibody (clone 4H8, Active Motif) using 7-day-old wild-type and *elf7-3* seedlings grown
361 under standard conditions. Library preparation and sequencing were performed by the
362 Epigenomics platform at IPS2 (Paris, France).
363
364 **ChIP-seq analysis**
365 The quality of ChIP-seq reads was first assessed using FastQC v0.11.9. Low-quality bases
366 and Illumina adapters were trimmed using cutadapt v4.2 with options "-q 15,10 -a
367 AGATCGGAAGAGCACACGTCTGAACTCCAGTCA -m 20". Clean reads were then aligned to
368 the TAIR10 reference genome using bowtie2 v2.5.1 (Langmead and Salzberg, 2012) with
369 the default parameters. Alignments were sorted by coordinate using the samtools sort
370 command from samtools v1.17 (Li et al., 2009). Duplicate reads were then marked using
371 the sambamba markdup command from sambamba v1.0 (Tarasov et al., 2015) and
372 uniquely mapped reads were retained using the samtools view command with options
373 "-F 4 -F 1024 -q 5". Coverage files in bedGraph format were obtained using the
374 genomeCoverageBed command from bedtools v2.31.0 (Quinlan, 2014) with options "-
375 bga -fs 200", and then these were converted to bigwig using the bedGraphToBigWig
376 command. Bigwigs were normalized to Counts Per Million (CPM) using the wiggletools
377 scale command from wiggletools v1.2 (Zerbino et al., 2014). Mean coverages of
378 biological replicates from each condition were obtained using the wiggletools mean

379 command. Log2 ratios between treatments and controls were obtained using the
380 bigwigCompare command from deeptools v3.5.1 (Ramírez et al., 2014).
381 Peak calling was performed over uniquely mapped reads using macs2 callpeak from
382 macs2 v2.2.7.1 (Zhang et al., 2008) with the following parameters: "--keep-dup all --
383 broad --broad-cutoff 0.05 -q 0.01 --nomodel --extsize 200". Peaks from biological
384 replicates were pooled and merged into a consensus set using the bedtools merge
385 command from bedtools v2.31.0 (Quinlan, 2014). In experiments that included various
386 treatments (ChIP-seq of H2Bub and RNAPII), the consensus peaks were obtained by
387 merging the peaks from each treatment using the same procedure as for the biological
388 replicates. Consensus peaks were annotated to their closest gene using the bedtools
389 closest command. To determine which genes could be considered as targets, the
390 following filters were applied: the peak must overlap more than half of the gene body,
391 or the gene body must overlap more than half of the peak, or the peak center must be
392 less than 200 pb away from the TSS.
393
394 **ChIP-Rx analysis**
395 H2Bub ChIP-Rx reads were first processed the same way as ChIP-seq reads. Clean reads
396 were aligned against a chimeric genome that contained both *Arabidopsis* (TAIR10) and
397 *Drosophila* (dm6) chromosomes. Alignments were sorted and duplicate-marked as in
398 ChIP-seq, and then reads that mapped to TAIR10 or to dm6 were separated. TAIR10
399 alignments were filtered and used to create coverage bigwigs and for peak calling as
400 previously described. Rx normalization factors were calculated as described in
401 Nassrallah et al., (2018). Briefly, the normalization factor α for each ChIP sample was
402 obtained using the following formula:
403 $$\alpha = \frac{r}{N_d IP}$$
404 where N_d is the number of mapped reads to *Drosophila* dm6 in millions and r is the
405 percentage of dm6 reads in the corresponding input sample. Hence, r was calculated as:
406 $$r = \frac{N_d i}{(N_d i + N_a i)} \times 100$$
407 where N_di and N_ai are the number of reads mapped to dm6 and TAIR10.

408 To test differential ubiquitination, read counts over the consensus H2Bub peaks
409 were first obtained using the multiBamSummay command from deeptools v3.5.1
410 (Ramírez et al., 2014) with options "--extendReads 200 --minMappingQuality 5". Gene
411 level counts were obtained by summing counts from peaks that were annotated to the
412 same gene. Differential analyses were performed using DESeq2 v1.38.0 (Love et al.,
413 2014). In these analyses, the Rx normalization factors were provided as size factors.
414 Genes showing an adjusted p-value inferior to 0.05 were considered as differentially
415 ubiquitinated.
416
417 **Pausing index**
418 To estimate RNAPII pausing, the pausing index formula was employed (Wang et al.,
419 2023a):
420 $$PI = \frac{TSS_{counts}/TSS_{length}}{GeneBody_{counts}/GeneBody_{length}}$$
421 The TSS was defined as a 400 pb region centered in the annotated TSS, whereas the
422 gene body spanned from the TSS region to the annotated TES. For this reason, only
423 RNAPII genes that were longer than 200 pb were included. Bedfiles of TSSs and gene
424 bodies were created using the slopBed command from bedtools v2.31.0 (Quinlan, 2014)
425 and the TAIR10 reference annotation. Counts over these regions were then obtained
426 using the multiBamSummary command from deeptools v3.5.1 (Ramírez et al., 2014).
427
428 **Re-analysis of existing datasets**
429 ChIP-seq reads of H3, H3K4me3, H3K36me3, H3K27me3, and H2A.Z (GSE231408;
430 samples GSM7075958, GSM7075959, GSM7075961, GSM7075962, GSM7075963,
431 GSM7075964, GSM7075985, GSM7075986 and GSM7075990) (Jamge et al., 2023) were
432 analysed as described in ChIP-seq analysis. MNase-seq reads of wild type Col-0
433 (GSE205110; samples GSM6205325 and GSM6205326) (Diego-Martín et al., 2022) were
434 downloaded, processed and aligned as described in ChIP-seq analysis. Coverage bigwigs
435 were obtained using DANPOS v2.2.2 (Chen et al., 2013) and the wigToBigWig command.
436
437 **Data representations**

438 Graphs were plotted in R 4.1.2 using ggplot2, eulerr and ComplexHeatmap libraries (Gu
439 et al., 2016). Other heatmaps and metaplots were obtained using the computeMatrix,
440 plotHeatmap and plotProfile commands from deeptools v3.5 (Ramírez et al., 2014).
441
442 **Subcellular fractionation**
443 Cytoplasmic, nucleoplasmic, and chromatin-associated fractions were obtained
444 following a described protocol (Liu et al., 2018), with some minor modifications. Briefly,
445 approximately 1.5 g of 7-day-old seedlings were ground in liquid nitrogen and
446 subsequently homogenized in 3-4 mL of Honda buffer (0.44 M Sucrose, 20 mM HEPES
447 KOH pH 7.4, 2.5% Percoll, 5% Dextran T40, 10 mM $MgCl_2$, 0.5% Triton X-100, 5mM DTT,
448 1 mM PMSF, and 1x protease inhibitor cocktail [cOmplete, EDTA-free; Roche]). The
449 resulting homogenate was filtered through two layers of Miracloth, and the flow-
450 through was then subjected to centrifugation at 2,400 *g* for 10 minutes at 4ºC. The
451 resulting supernatant (1 mL) was further centrifuged at 10,000g for 10 minutes at 4ºC,
452 and this supernatant was collected as the cytoplasmic fraction. The pellet was
453 resuspended in 1 mL of Honda buffer and centrifuged at 1,800 *g* for 5 minutes at 4ºC to
454 concentrate nuclei. This pellet was subsequently washed 4-6 times with Honda buffer
455 and rinsed with PBS buffer (137 mM NaCl, 2.7 mM KCl, 10 mM Na_2HPO_4, and 2 mM
456 KH_2PO_4) containing 1 mM EDTA. The resulting pellet was resuspended in 150 µL of cold
457 glycerol buffer (20 mM Tris-HCl pH 7.9, 50% glycerol, 75 mM NaCl, 0.5 mM EDTA, 0.85
458 mM DTT, 0.125 mM PMSF, and 1x protease inhibitor cocktail [cOmplete, EDTA-free;
459 Roche]) and gently vortexed twice after adding 150 µL of cold nuclei lysis buffer (10 mM
460 HEPES KOH pH 7.4, 7.5 mM $MgCl_2$, 0.2 mM EDTA, 0.3 M NaCl, 1 M urea, 1% NP-40, 1
461 mM DTT, 0.5 mM PMSF, 10 mM β-mercaptoethanol, and 1x protease inhibitor cocktail
462 [cOmplete, EDTA-free; Roche]). The mixture was then incubated for 2 minutes on ice
463 and centrifuged at 14,000 rpm for 2 minutes at 4ºC. The resulting supernatant was
464 collected as the nucleoplasmic fraction. The chromatin-associated pellet was rinsed with
465 PBS buffer containing 1 mM EDTA and then resuspended in 150 µL of cold glycerol buffer
466 plus 150 µL of cold nuclei lysis buffer. Protein concentrations were determined using the
467 Pierce 660 nm Protein Assay following the manufacturer's instructions. The various
468 fractions were subsequently analyzed by immunoblot.
469

470 **Immunoblot analysis**

471 Total protein extracts and subcellular fractionation samples were separated with SDS-
472 PAGE, transferred to PVDF membranes, and immunolabeled with commercial
473 antibodies against histone H3 (ab1791, Abcam) and against tubulin (62204, Invitrogen).
474 Chemiluminescence was detected using the Supersignal west FEMTO substrate with
475 maximum sensitivity (Thermo-Fisher Scientific), and protein bands were detected and
476 quantified using the LAS-3000 Imaging System (Fujifilm) and ImageJ software,
477 respectively. The custom-made rabbit anti-HUB1 antibody was generated for F.
478 Barneche by SDIX (Newark, USA) using the following immunogen sequence
479 MQDTLLIDKYIMDKDIQQGSAYASFLSKKSSRIEDQLRFCTDQFQKLAEDKYQKSVSLENL
480 QKKRADIGNGLEQARSRLEESHSKVEQSRLDYGALELEL.

481

482 **ACCESSION NUMBERS**

483 The sequencing data generated in this work have been deposited in the GEO public
484 functional genomics data repository under the accession number GSE244850. The
485 following secure token has been created to allow review of record GSE244850 while it
486 remains in private status: "ezozkoowltshtox".

487

488 **SUPPLEMENTAL DATA**

489 Supplemental document 1: Supplemental Figures S1-S5.

490 Supplemental document 2: Supplemental Table.

491

492 **ACKNOWLEDGEMENTS AND FUNDING**

493 We thank Christian S. Hardtke (University of Lausanne, Switzerland) and Ligeng Ma
494 (Capital Normal University, China) for sharing seeds of the *35S:GFP-VIP3* line and of *elf7-*
495 *3* and *pELF7:Flag-ELF7 elf7-3*, respectively. N.B-T was supported by a predoctoral
496 contract from the MINECO [BES-2014-068868] and an EMBO Short-Term fellowship (STF
497 n°8047) to visit the Barneche/Bourbousse laboratory. J.P-A was supported by a
498 predoctoral contract from the Generalitat Valenciana (CIACIF/2021/432). Research in
499 the IBMCP laboratories was funded by grants BIO2013-43184-P (to M.A.B. and D.A.) and
500 BIO2016-79133-P (to D.A.) from the Spanish Ministry of Economy and Innovation, as
501 well as grants PID2019-109925GB-I00 (to D.A.) and RYC2018-024108-I and PID2019-

502 108577GA-I00 (to J.G-B) from MCIN/AEI/10.13039/501100011033. Research in the
503 Barneche/Bourbousse laboratory was funded by Agence Nationale de la Recherche
504 grants ChromaLight (ANR-18-CE13-0004-01), Epilinks (ANR-22-CE20-0001) and
505 PlastoNuc (ANR-20-CE13-0028). Research in the Benhamed laboratory was funded by
506 the European Research Council ERC (Project 101044399-3Dwheat), Agence National de
507 la Recherche ANR (ANR-21-CE20-0036-4D Heat Tomato) and by the Institut Universitaire
508 de France (IUF).
509

510 **AUTHOR CONTRIBUTIONS**

511 N.B-T., J.P-A., C.B., M.B., F.B., M.A.B., J.G-B., and D.A. designed the research; N.B-T., J.P-
512 A., C.B., D.L., O.A., M.B., F.B., J.G-B., and D.A. performed research; N.B-T., J.P-A., C.B.,
513 D.L., O.A., M.B., F.B., M.A.B., J.G-B., and D.A. analyzed data; D.A. wrote the paper.
514

515 **REFERENCES**

516 **Antosz W, Pfab A, Ehrnsberger HF, Holzinger P, Kollen K, Mortensen SA, Bruckmann**
517 **A, Schubert T, Langst G, Griesenbeck J, et al** (2017) The Composition of the
518 Arabidopsis RNA Polymerase II Transcript Elongation Complex Reveals the
519 Interplay between Elongation and mRNA Processing Factors. Plant Cell **29**: 854–
520 870

521 **Bourbousse C, Ahmed I, Roudier F, Zabulon G, Blondet E, Balzergue S, Colot V,**
522 **Bowler C, Barneche F** (2012) Histone H2B monoubiquitination facilitates the rapid
523 modulation of gene expression during Arabidopsis photomorphogenesis. PLoS
524 Genet **8**: e1002825

525 **Cao Y, Wen L, Wang Z, Ma L** (2015) SKIP Interacts with the Paf1 Complex to Regulate
526 Flowering via the Activation of FLC Transcription in Arabidopsis. Mol Plant **8**:
527 1816–1819

528 **Chen F, Woodfin A, Gardini A, Rickels R, Marshall S, Smith E, Shiekhattar R,**
529 **Shilatifard A** (2015) PAF1, a Molecular Regulator of Promoter-Proximal Pausing by
530 RNA Polymerase II. Cell **162**: 1003–1015

531 **Chen K, Xi Y, Pan X, Li Z, Kaestner K, Tyler J, Dent S, He X, Li W** (2013) DANPOS:
532 Dynamic analysis of nucleosome position and occupancy by sequencing. Genome
533 Res **23**: 341–351

534 **Coleman-Derr D, Zilberman D** (2012) Deposition of histone variant H2A.Z within gene
535 bodies regulates responsive genes. PLoS Genet **8**: e1002988
536 **Diego-Martín B, Pérez-Alemany JP, Candela-Ferré J, Corbalán-Acedo A, Pereyra J,**
537 **Alabadí D, Jami-Alahmadi Y, Wohlschlegel J, Gallego-Bartolomé J** (2022) The
538 TRIPLE PHD FINGERS proteins are required for SWI/SNF complex-mediated +1
539 nucleosome positioning and transcription start site determination in Arabidopsis.
540 Nucleic Acids Res **50**: 10399–10417
541 **Dobin A, Davis CA, Schlesinger F, Drenkow J, Zaleski C, Jha S, Batut P, Chaisson M,**
542 **Gingeras TR** (2013) STAR: Ultrafast universal RNA-seq aligner. Bioinformatics **29**:
543 15–21
544 **Dorcey E, Rodriguez-Villalon A, Salinas P, Santuari L, Pradervand S, Harshman K,**
545 **Hardtke CS** (2012) Context-dependent dual role of SKI8 homologs in mRNA
546 synthesis and turnover. PLoS Genet **8**: e1002652
547 **Fal K, Cortes M, Liu M, Collaudin S, Das P, Hamant O, Trehin C** (2019) Paf1c defects
548 challenge the robustness of flower meristem termination in Arabidopsis thaliana.
549 Development **146**: dev173377
550 **Fal K, Liu M, Duisembekova A, Refahi Y, Haswell ES, Hamant O** (2017) Phyllotactic
551 regularity requires the paf1 complex in Arabidopsis. Development **144**: 4428–
552 4436
553 **Francette AM, Tripplehorn SA, Arndt KM** (2021) The Paf1 Complex: A Keystone of
554 Nuclear Regulation Operating at the Interface of Transcription and Chromatin. J
555 Mol Biol **433**: 166979
556 **Gómez-Zambrano Á, Merini W, Calonje M** (2019) The repressive role of Arabidopsis
557 H2A.Z in transcriptional regulation depends on AtBMI1 activity. Nat Commun **10**:
558 2828
559 **Gu Z, Eils R, Schlesner M** (2016) Complex heatmaps reveal patterns and correlations in
560 multidimensional genomic data. Bioinformatics **32**: 2847–2849
561 **He Y, Doyle MR, Amasino RM** (2004) PAF1-complex-mediated histone methylation of
562 FLOWERING LOCUS C chromatin is required for the vernalization-responsive,
563 winter-annual habit in Arabidopsis. Genes Dev **18**: 2774–2784
564 **Hou L, Wang Y, Liu Y, Zhang N, Shamovsky I, Nudler E, Tian B, Dynlacht BD** (2019)
565 Paf1C regulates RNA polymerase II progression by modulating elongation rate.

566 Proc Natl Acad Sci U S A **116**: 14583–14592
567 **Jamge B, Lorković ZJ, Axelsson E, Osakabe A, Shukla V, Yelagandula R, Akimcheva S,**
568 **Kuehn AL, Berger F, Biocenter V, et al** (2023) Histone variants shape chromatin
569 states in Arabidopsis. Elife **12**: RP87714
570 **Kim J, Roeder RG** (2009) Direct Bre1-Paf1 complex interactions and RING finger-
571 independent Bre1-Rad6 interactions mediate histone H2B ubiquitylation in yeast.
572 J Biol Chem **284**: 20582–20592
573 **Kindgren P, Ivanov M, Marquardt S** (2019) Native elongation transcript sequencing
574 reveals temperature dependent dynamics of nascent RNAPII transcription in
575 Arabidopsis. Nucleic Acids Res. doi: 10.1093/nar/gkz1189
576 **Langmead B, Salzberg SL** (2012) Fast gapped-read alignment with Bowtie 2. Nat
577 Methods **9**: 357–359
578 **Li C, Guo Y, Wang L, Yan S** (2023) The SMC5 /6 complex recruits the PAF1 complex to
579 facilitate DNA double-strand break repair in Arabidopsis. EMBO J **42**: e112756
580 **Li H, Handsaker B, Wysoker A, Fennell T, Ruan J, Homer N, Marth G, Abecasis G,**
581 **Durbin R** (2009) The Sequence Alignment/Map format and SAMtools.
582 Bioinformatics **25**: 2078–2079
583 **Li R, Wei Z, Li Y, Shang X, Cao Y, Duan L, Ma L** (2022) SKI-INTERACTING PROTEIN
584 interacts with SHOOT MERISTEMLESS to regulate shoot apical meristem
585 formation. Plant Physiol **189**: 2193–2209
586 **Li Y, Yang J, Shang X, Lv W, Xia C, Wang C, Feng J, Cao Y, He H, Li L, et al** (2019) SKIP
587 regulates environmental fitness and floral transition by forming two distinct
588 complexes in Arabidopsis. New Phytol **224**: 321–335
589 **Liao Y, Smyth GK, Shi W** (2014) FeatureCounts: An efficient general purpose program
590 for assigning sequence reads to genomic features. Bioinformatics **30**: 923–930
591 **Liu C, Xin Y, Xu L, Cai Z, Xue Y, Liu Y, Xie D, Liu Y, Qi Y** (2018) Arabidopsis ARGONAUTE
592 1 Binds Chromatin to Promote Gene Transcription in Response to Hormones and
593 Stresses. Dev Cell **44**: 348-361 e7
594 **Liu Y, Geyer R, van Zanten M, Carles A, Li Y, Horold A, van Nocker S, Soppe WJ** (2011)
595 Identification of the Arabidopsis REDUCED DORMANCY 2 gene uncovers a role for
596 the polymerase associated factor 1 complex in seed dormancy. PLoS One **6**:
597 e22241

598 **Liu Y, Koornneef M, Soppe WJ** (2007) The absence of histone H2B monoubiquitination
599 in the Arabidopsis hub1 (rdo4) mutant reveals a role for chromatin remodeling in
600 seed dormancy. Plant Cell **19**: 433–444
601 **Love MI, Huber W, Anders S** (2014) Moderated estimation of fold change and
602 dispersion for RNA-seq data with DESeq2. Genome Biol **15**: 1–21
603 **Lu C, Tian Y, Wang S, Su Y, Mao T, Huang T, Chen Q, Xu Z, Ding Y** (2017)
604 Phosphorylation of SPT5 by CDKD;2 Is Required for VIP5 Recruitment and Normal
605 Flowering in Arabidopsis thaliana. Plant Cell **29**: 277–291
606 **Mayer A, Lidschreiber M, Siebert M, Leike K, Söding J, Cramer P** (2010) Uniform
607 transitions of the general RNA polymerase II transcription complex. Nat Struct
608 Mol Biol **17**: 1272–1278
609 **Nagaike T, Logan C, Hotta I, Rozenblatt-Rosen O, Meyerson M, Manley JL** (2011)
610 Transcriptional Activators Enhance Polyadenylation of mRNA Precursors. Mol Cell
611 **41**: 409–418
612 **Nasim Z, Susila H, Jin S, Youn G, Ahn JH** (2022) Polymerase II–Associated Factor 1
613 Complex-Regulated FLOWERING LOCUS C-Clade Genes Repress Flowering in
614 Response to Chilling. Front Plant Sci **13**: 817356
615 **Nassrallah A, Rougee M, Bourbousse C, Drevensek S, Fonseca S, Iniesto E, Ait-**
616 **Mohamed O, Deton-Cabanillas AF, Zabulon G, Ahmed I, et al** (2018) DET1-
617 mediated degradation of a SAGA-like deubiquitination module controls H2Bub
618 homeostasis. Elife **7**: e37892
619 **Ng HH, Dole S, Struhl K** (2003) The Rtf1 Component of the Paf1 Transcriptional
620 Elongation Complex Is Required for Ubiquitination of Histone H2B. J Biol Chem
621 **278**: 33625–33628
622 **Obermeyer S, Kapoor H, Markusch H, Grasser KD** (2023) Transcript elongation by RNA
623 polymerase II in plants: factors, regulation and impact on gene expression. Plant J
624 10.1111/tpj.16115
625 **Obermeyer S, Stöckl R, Schnekenburger T, Moehle C, Schwartz U, Grasser KD** (2022)
626 Distinct role of subunits of the Arabidopsis RNA polymerase II elongation factor
627 PAF1C in transcriptional reprogramming. Front Plant Sci **13**: 974625
628 **Oh S, Park S, van Nocker S** (2008) Genic and global functions for Paf1C in chromatin
629 modification and gene expression in Arabidopsis. PLoS Genet **4**: e1000077

630 **Oh S, Zhang H, Ludwig P, van Nocker S** (2004) A mechanism related to the yeast
631 transcriptional regulator Paf1c is required for expression of the Arabidopsis
632 FLC/MAF MADS box gene family. Plant Cell **16**: 2940–2953
633 **Park S, Oh S, Ek-Ramos J, van Nocker S** (2010) PLANT HOMOLOGOUS TO
634 PARAFIBROMIN is a component of the PAF1 complex and assists in regulating
635 expression of genes within H3K27ME3-enriched chromatin. Plant Physiol **153**:
636 821–831
637 **Quinlan AR** (2014) BEDTools: The Swiss-Army tool for genome feature analysis. Curr
638 Protoc Bioinforma. doi: 10.1002/0471250953.bi1112s47
639 **Rahl PB, Lin CY, Seila AC, Flynn RA, McCuine S, Burge CB, Sharp PA, Young RA** (2010)
640 c-Myc regulates transcriptional pause release. Cell **141**: 432–445
641 **Ramírez F, Dündar F, Diehl S, Grüning BA, Manke T** (2014) DeepTools: A flexible
642 platform for exploring deep-sequencing data. Nucleic Acids Res **42**: 187–191
643 **Rondón AG, Gallardo M, García-Rubio M, Aguilera A** (2004) Molecular evidence
644 indicating that the yeast PAF complex is required for transcription elongation.
645 EMBO Rep **5**: 47–53
646 **Roudier F, Ahmed I, Bérard C, Sarazin A, Mary-Huard T, Cortijo S, Bouyer D, Caillieux**
647 **E, Duvernois-Berthet E, Al-Shikhley L, et al** (2011) Integrative epigenomic
648 mapping defines four main chromatin states in Arabidopsis. EMBO J **30**: 1928–
649 1938
650 **Schmitz RJ, Tamada Y, Doyle MR, Zhang X, Amasino RM** (2009) Histone H2B
651 deubiquitination is required for transcriptional activation of FLOWERING LOCUS C
652 and for proper control of flowering in Arabidopsis. Plant Physiol **149**: 1196–1204
653 **Shi X, Chang M, Wolf AJ, Chang CH, Frazer-Abel AA, Wade PA, Burton ZF, Jaehning JA**
654 (1997) Cdc73p and Paf1p are found in a novel RNA polymerase II-containing
655 complex distinct from the Srbp-containing holoenzyme. Mol Cell Biol **17**: 1160–
656 1169
657 **Tarasov A, Vilella AJ, Cuppen E, Nijman IJ, Prins P** (2015) Sambamba: Fast processing
658 of NGS alignment formats. Bioinformatics **31**: 2032–2034
659 **Vos SM, Farnung L, Boehning M, Wigge C, Linden A, Urlaub H, Cramer P** (2018)
660 Structure of activated transcription complex Pol II–DSIF–PAF–SPT6. Nature **560**:
661 607–612

662 **Vos SM, Farnung L, Linden A, Urlaub H, Cramer P** (2020) Structure of complete Pol II–
663 DSIF–PAF–SPT6 transcription complex reveals RTF1 allosteric activation. Nat
664 Struct Mol Biol **27**: 668–677
665 **Wang H, Fan Z, Shliaha P V, Miele M, Hendrickson RC, Jiang X, Helin K** (2023a)
666 H3K4me3 regulates RNA polymerase II promoter-proximal pause-release. Nature
667 **615**: 339
668 **Wang M, Zhong Z, Gallego-Bartolomé J, Li Z, Feng S, Kuo HY, Kan RL, Lam H, Richey**
669 **JC, Tang L, et al** (2023b) A gene silencing screen uncovers diverse tools for
670 targeted gene repression in Arabidopsis. Nat Plants **9**: 460–472
671 **Wood A, Schneider J, Dover J, Johnston M, Shilatifard A** (2003) The Paf1 complex is
672 essential for histone monoubiquitination by the Rad6-Bre1 complex, which signals
673 for histone methylation by COMPASS and Dot1p. J Biol Chem **278**: 34739–34742
674 **Wu L, Li L, Zhou B, Qin Z, Dou Y** (2014) H2B ubiquitylation promotes RNA Pol II
675 processivity via PAF1 and pTEFb. Mol Cell **54**: 920–931
676 **Yu M, Yang W, Ni T, Tang Z, Nakadai T, Zhu J, Roeder RG** (2015) RNA polymerase II-
677 associated factor 1 regulates the release and phosphorylation of paused RNA
678 polymerase II. Science (80-) **350**: 1383–1386
679 **Yu X, Michaels SD** (2010) The Arabidopsis Paf1c complex component CDC73
680 participates in the modification of FLOWERING LOCUS C chromatin. Plant Physiol
681 **153**: 1074–1084
682 **Zerbino DR, Johnson N, Juettemann T, Wilder SP, Flicek P** (2014) WiggleTools: Parallel
683 processing of large collections of genome-wide datasets for visualization and
684 statistical analysis. Bioinformatics **30**: 1008–1009
685 **Zhang H, Li X, Song R, Zhan Z, Zhao F, Li Z, Jiang D** (2022) Cap-binding complex assists
686 RNA polymerase II transcription in plant salt stress response. Plant Cell Environ
687 **45**: 2780–2793
688 **Zhang H, Van Nocker S** (2002) The Vernalization Independence 4 gene encodes a novel
689 regulator of Flowering Locus C. Plant J **31**: 663–673
690 **Zhang H, Ransom C, Ludwig P, Van Nocker S** (2003) Genetic analysis of early flowering
691 mutants in Arabidopsis defines a class of pleiotropic developmental regulator
692 required for expression of the flowering-time switch FLOWERING LOCUS C.
693 Genetics **164**: 347–358

694 **Zhang Y, Liu T, Meyer CA, Eeckhoute J, Johnson DS, Bernstein BE, Nussbaum C, Myers**
695 **RM, Brown M, Li W, et al** (2008) Model-based analysis of ChIP-Seq (MACS).
696 Genome Biol **9**: R137
697 **Zhao F, Xue M, Zhang H, Li H, Zhao T, Jiang D** (2023) Coordinated histone variant
698 H2A.Z eviction and H3.3 deposition control plant thermomorphogenesis. New
699 Phytol **238**: 750–764
700
701 **FIGURE LEGENDS**
702 **Figure 1.** ELF7 and VIP3 bind to the gene body of transcribed genes. **A)** Venn diagram
703 showing the overlap between Flag-ELF7 and GFP-VIP3 peaks. **B)** The heatmap shows the
704 occupancy of Flag-ELF7, GFP-VIP3, and total RNAPII ranked by the decreasing Flag-ELF7
705 level. **C, D)** Average occupancy of Flag-ELF7 (C) and GFP-VIP3 (D) on target genes ranked
706 by their expression level. **E, F)** MA plot with DEGs (*p* adj. < 0.05) in the *elf7-3* mutant
707 compared with wild type for Paf1C target genes (E) and for genes in which we could not
708 detect Paf1C (F).
709
710 **Figure 2.** The H2Bub mark is reduced in *elf7-3* mutants.**A)** Average occupancy of the
711 H2Bub mark in the wild type and in the *elf7-3* mutant. **B)** Heatmaps showing Flag-ELF7,
712 H2Bub -in wild-type and *elf7-3* seedlings- and RNAPII occupancy in gene clusters based
713 on H2Bub and Paf1C, H2Bub, or Paf1C occupancy. Genes are ranked by their decreasing
714 levels of H2Bub in wild type. **C)** The MA plot shows differentially ubiquitinated genes
715 (blue dots; *p* adj. < 0.05) between the wild type and the *elf7-3* mutant.
716
717 **Figure 3.** The recruitment of HUB1 and HUB2 to chromatin is independent of Paf1C. **A)**
718 Immunoblot showing the specificity of the antiserum raised against HUB1 and HUB2.
719 The bottom panels show the Ponceau staining. **B)** Detection of HUB1/HUB2 in
720 cytoplasmic, nucleosplasmic, and chromatin fractions by Western blot analysis. Histone
721 H3 was used as a chromatin marker and tubulin and Ponceau staining as cytoplasmic
722 markers. The position of the molecular weight markers is shown on the right. The
723 asterisk marks a non-specific band detected with the anti-tubulin antibody.
724
725 **Figure 4.** HUB1 and ELF7 regulate a common set of genes. **A)** MA plot showing DEGs (*p*

726 adj. < 0.05) between *hub1-4* and wild-type seedlings. **B)** Comparison of DEGs between
727 *hub1-4* and *elf7-3* seedlings. **C)** Scatter plot showing the correlation of common DEGs
728 between *hub1-4* and *elf7-3* mutant seedlings. **D)** The heatmap shows the behavior of
729 common DEGs between *hub1-4* and *elf7-3* mutant seedlings.
730
731 **Figure 5.** RNAPII genomic distribution is affected in *elf7-3* seedlings. **A)** The metagene
732 analysis shows the average distribution of all RNAPII-occupied genes in wild type and in
733 *elf7-3* mutants. **B)** Average distributions of RNAPII in wild type and *elf7-3* seedlings
734 centered on the TSS, and compared with the nucleosome position previously
735 determined by MNase-seq (Diego-Martín et al., 2022). **C)** The heatmap shows the effect
736 of the *elf7-3* mutation on the distribution of RNAPII and H2Bub in genes occupied by
737 Paf1C (Paf1C targets) and in genes in which we could not detect binding of Paf1C (Other
738 RNAPII). **D)** Scheme depicting the calculation used to determine the pausing index (PI).
739 **E)** Representation of the PI in wild type and *elf7-3* mutant. The higher the PI, the greater
740 the degree of paused RNAPII.

Figure 1

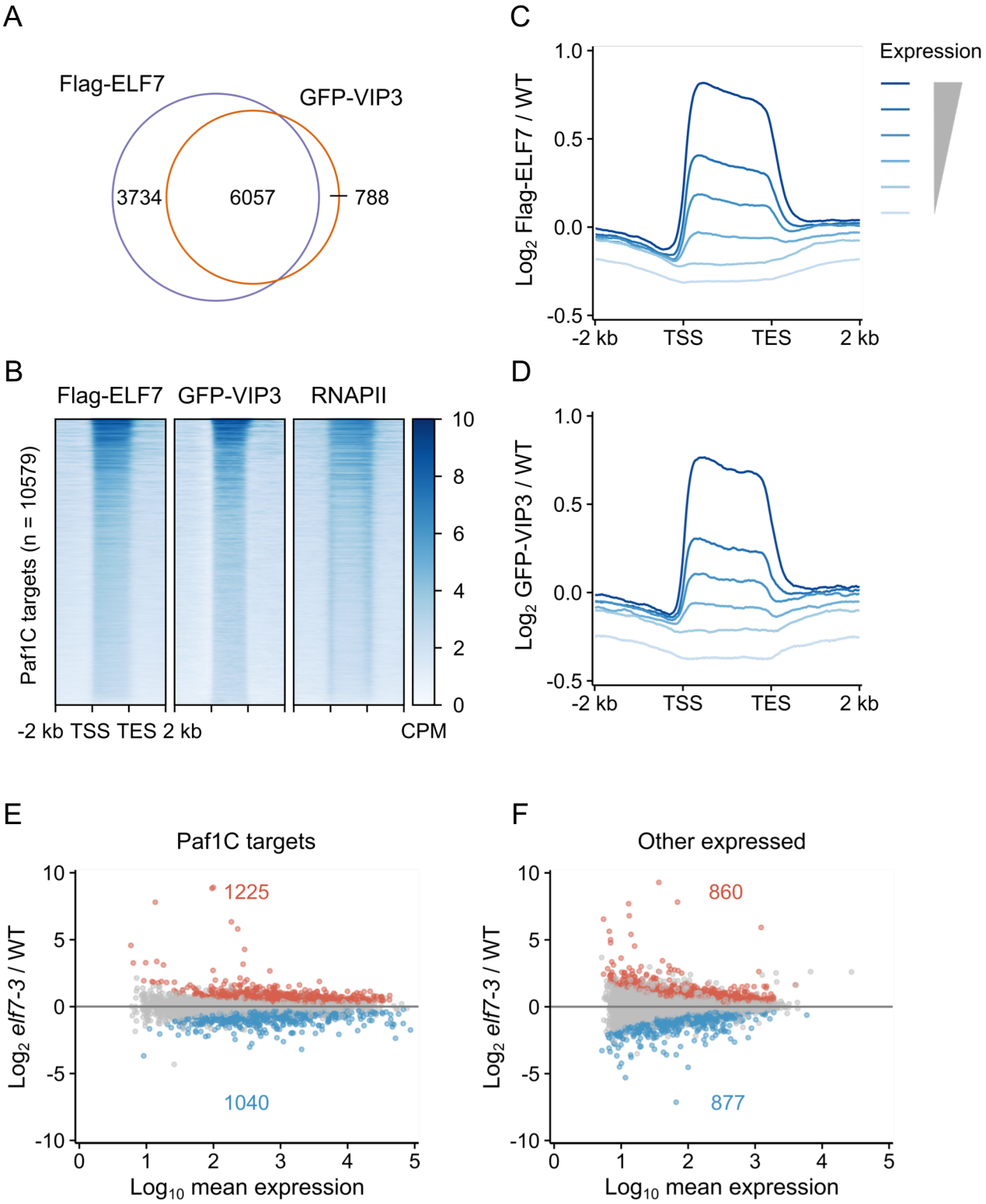
A
Flag-ELF7
GFP-VIP3
3734
6057
788
B
Flag-ELF7
GFP-VIP3
RNAPII
Paf1C targets (n = 10579)
-2 kb TSS TES 2 kb
CPM
10
8
6
4
2
0
C
Expression
Log2 Flag-ELF7 / WT
1.0
0.5
0.0
-0.5
-2 kb
TSS
TES
2 kb
D
Log2 GFP-VIP3 / WT
1.0
0.5
0.0
-0.5
-2 kb
TSS
TES
2 kb
E
Paf1C targets
1225
1040
Log2 elf7-3 / WT
10
5
0
-5
-10
0
1
2
3
4
5
Log10 mean expression
F
Other expressed
860
877
Log2 elf7-3 / WT
10
5
0
-5
-10
0
1
2
3
4
5
Log10 mean expression

Figure 2

A

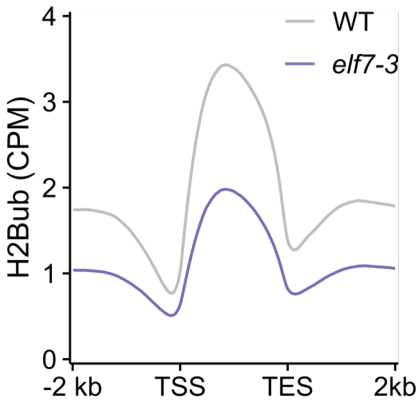
WT
elf7-3
H2Bub (CPM)
4
3
2
1
0
-2 kb
TSS
TES
2kb

C

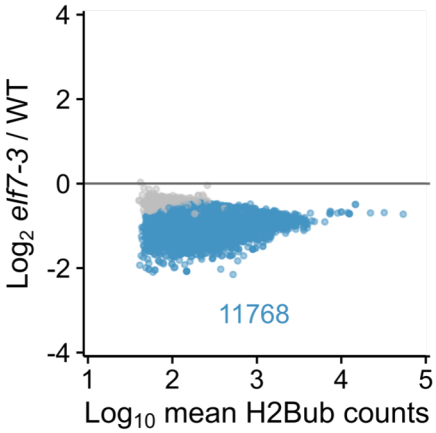
Log2 elf7-3 / WT
4
2
0
-2
-4
11768
1
2
3
4
5
Log10 mean H2Bub counts

B

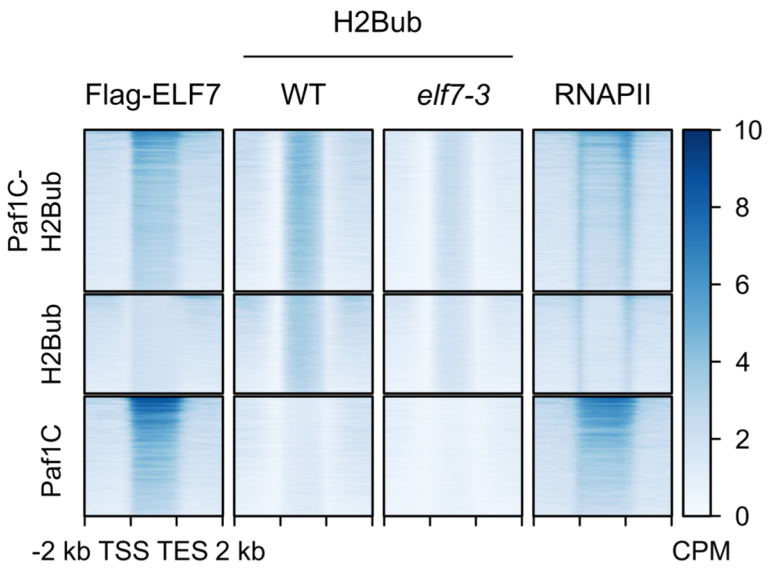
H2Bub
Flag-ELF7
WT
elf7-3
RNAPII
Paf1C-H2Bub
H2Bub
Paf1C
10
8
6
4
2
0
-2 kb TSS TES 2 kb
CPM

Figure 3

A

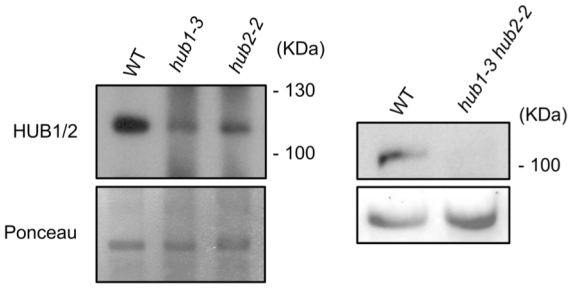
WT
hub1-3
hub2-2
(KDa)
- 130
HUB1/2
- 100
Ponceau
WT
hub1-3 hub2-2
(KDa)
- 100

B

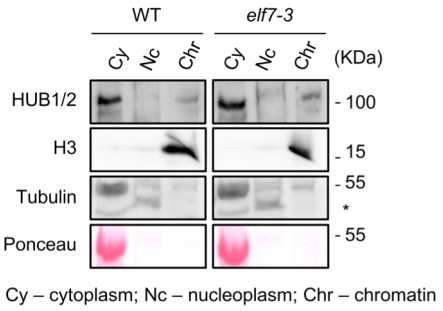
WT
elf7-3
Cy
Nc
Chr
Cy
Nc
Chr
(KDa)
HUB1/2
- 100
H3
- 15
Tubulin
- 55
*
Ponceau
- 55
Cy – cytoplasm; Nc – nucleoplasm; Chr – chromatin

Figure 4

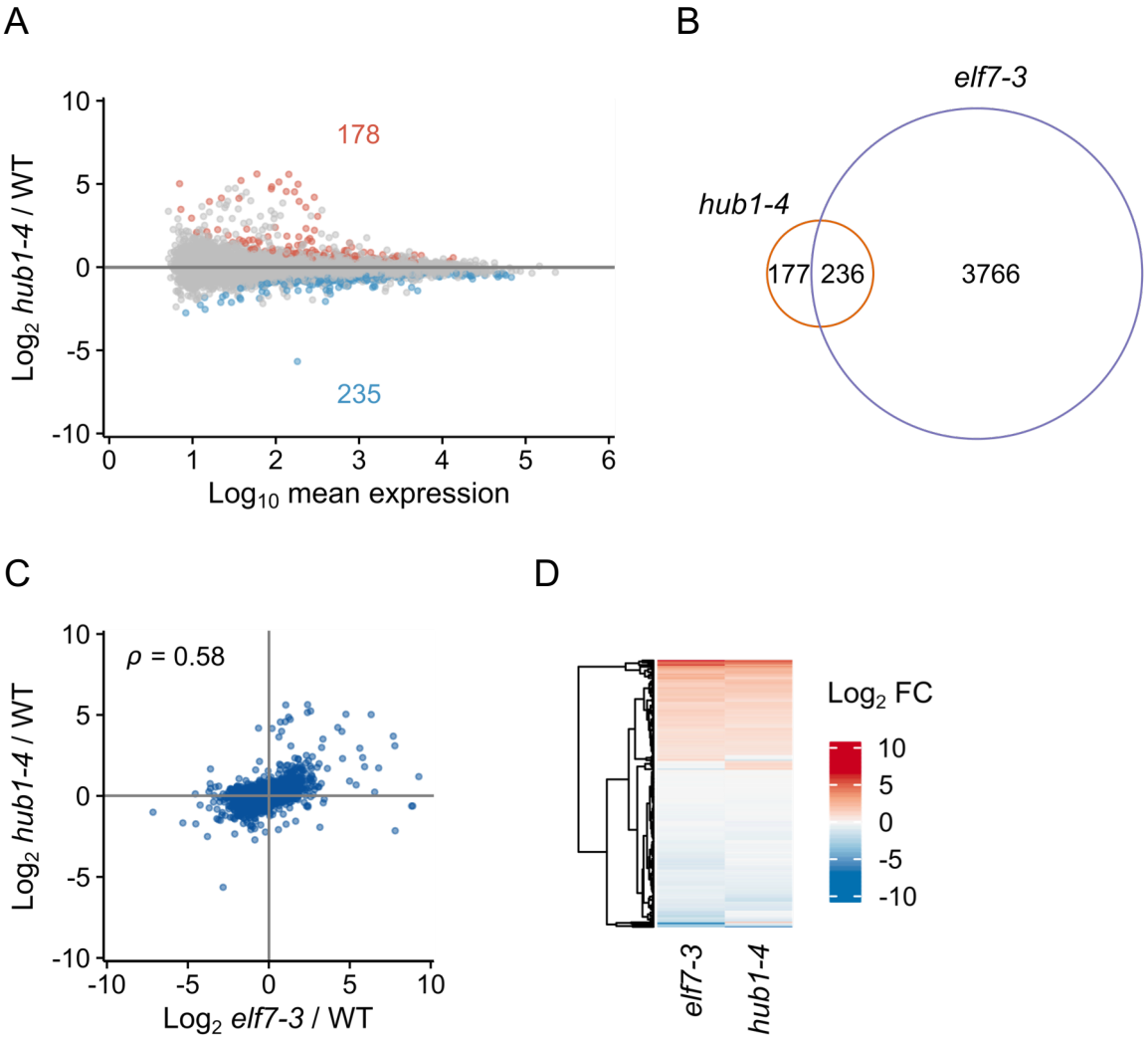
A
178
235
Log2 hub1-4 / WT
Log10 mean expression
B
elf7-3
hub1-4
177
236
3766
C
ρ = 0.58
Log2 hub1-4 / WT
Log2 elf7-3 / WT
D
Log2 FC
elf7-3
hub1-4

Figure 5

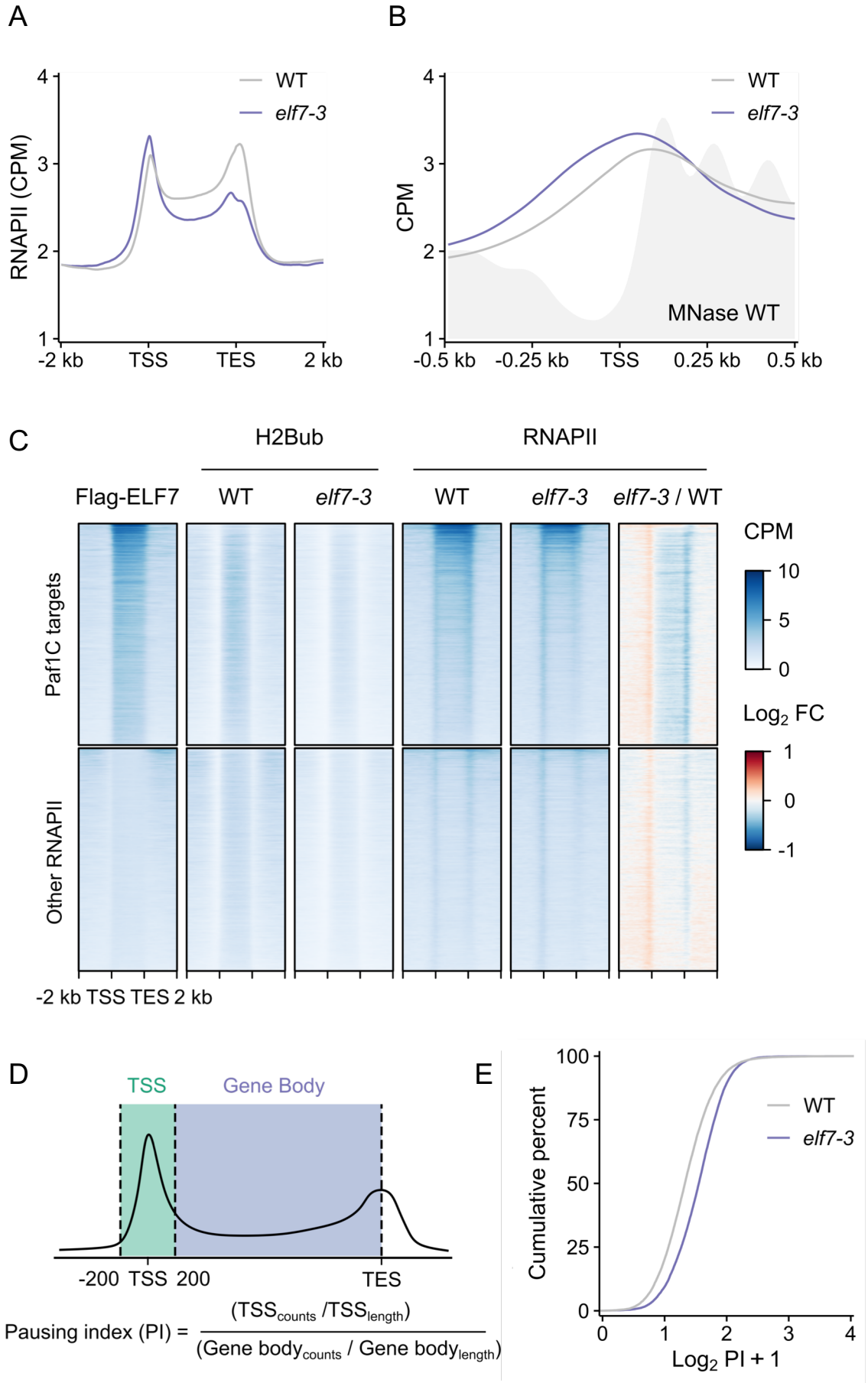
A
RNAPII (CPM)
WT
elf7-3
-2 kb
TSS
TES
2 kb
B
CPM
WT
elf7-3
MNase WT
-0.5 kb
-0.25 kb
TSS
0.25 kb
0.5 kb
C
H2Bub
RNAPII
Flag-ELF7
WT
elf7-3
WT
elf7-3
elf7-3 / WT
Paf1C targets
Other RNAPII
CPM
Log2 FC
-2 kb TSS TES 2 kb
D
TSS
Gene Body
-200 TSS 200
TES
Pausing index (PI) = (TSS counts / TSS length) / (Gene body counts / Gene body length)
E
Cumulative percent
WT
elf7-3
Log2 PI + 1